Inorganic Chemistry

Article

pubs.acs.org/IC

Metal–Organic Frameworks with Phosphotungstate Incorporated for Hydrolytic Cleavage of a DNA-Model Phosphodiester

Qiuxia Han,[†,‡] Lejie Zhang,[†] Cheng He,[†] Jiangyang Niu,[‡] and Chunying Duan*[,†]

[†]State Key Laboratory of Fine Chemicals, Dalian Technology of University, Dalian, 116023, People's Republic of China

[‡]School of Chemistry and Chemical Engineering, Henan University, Kaifeng, 475004, People's Republic of China

Supporting Information

ABSTRACT: Five phosphotungstate-incorporated metal–organic frameworks $\{[Eu_4(dpdo)_9(H_2O)_{16}PW_{12}O_{40}]\}$-$(PW_{12}O_{40})_2\cdot(dpdo)_3\cdot Cl_3$ (**1**); $\{ZnNa_2(\mu\text{-}OH)(dpdo)_4(H_2O)_4[PW_{12}O_{40}]\}\cdot 3H_2O$ (**2**); $\{Zn_3(dpdo)_7\}[PW_{12}O_{40}]_2\cdot 3H_2O$ (3); and $[Ln_2H(\mu\text{-}O)_2(dpdo)_4(H_2O)_2][PW_{12}O_{40}]\cdot 3H_2O$ (Ln = Ho for **4** and Yb for **5**) (dpdo = 4,4′-bipyridine-*N*,*N*′-dioxide) have been synthesized through a one-step hydrothermal reaction and characterized by elemental analyses, infrared (IR) spectroscopy, photoluminescence, and single-crystal X-ray diffraction (XRD). The structural analyses indicate that **1**–**5** display diversity structure from one-dimensional (1D) to three-dimensional (3D) series of hybrids. Kinetic experiments for the hydrolytic cleavage of DNA-model phosphodiester BNPP (bis(*p*-nitrophenyl)phosphate) were followed spectrophotometrically for the absorbance increase at 400 nm in EPPS (4-(2-hydroxyethyl)piperazine-1-propane sulfonic acid) buffer solution, because of the formation of *p*-nitrophenoxide with **1**–**5** under conditions of pH 4.0 and 50 °C. Ultraviolet (UV) spectroscopy indicate that the cleavage of the phosphodiester bond proceeds with the pseudo-first-order rate constant in the range of 10^{-7}–10^{-6} s^{-1}, giving an inorganic phosphate and *p*-nitrophenol as the final products of hydrolysis. The results demonstrate that **1**–**5** have good catalytic activity and reusability for hydrolytic cleavage of BNPP.

INTRODUCTION

The development of rational approaches to the design of catalysts for hydrolysis of phosphate diesters has attracted substantial research efforts in bio-organic chemistry in the last 20 years for the following reasons: (1) mechanistic information obtained in the study of artificial agents could lead to a better understanding of the chemistry of the corresponding hydrolytic enzymes, (2) efficient phosphate diester hydrolytic agents could be employed as artificial restriction enzymes for molecular biology, and (3) the realization of anti-DNA drugs can be envisaged in the more distant future.[1] The Lewis acidity of the trivalent and tetravalent lanthanide ions, together with their high coordination numbers, fast ligand-exchange rates, and absence of accessible redox chemistry, provides an opportunity to mimic the activity of hydrolases to bind and activate phosphate esters for cleavage.[2] Besides, Zn^{2+}, except for having the aforementioned characteristics, also has some features such as being nontoxic and having a ligand field stabilization energy; as a consequence, it is the only metal frequently encountered in both natural and artificial agents, and the development of Zn^{2+}-based artificial enzymes has been highly valued.[3] Since the first studies on DNA manipulation with artificial agents described in 2006,[4] considerable attention has been concentrated on homogeneous catalysts for the hydrolysis of phosphate diesters in an aqueous solution, despite the exceptional resistance of phosphate diesters to hydrolytic cleavage at neutral pH value. Mechanistic investigations, conducted by Komiyama, are in agreement with a concerted five-coordinate phosphate intermediate (or transition state).[5] Although significant potential advantages of heterogeneous catalysis, such as ease of separation, efficient recycling, and minimization of metal traces in the product,[6] heterogeneous catalysts for the hydrolysis of phosphate diesters are scarce.[7]

The design of active, environmentally benign, and recyclable heterogeneous catalysts is expected to have a major impact on the hydrolysis of phosphate diesters applications. Metal–organic frameworks (MOFs) have attracted considerable attention over recent years, because of their intriguing architectures and properties as well as potential applications in catalysis, magnetism, and sensitive devices.[8] Generally, one effective approach for novel hybrid assemblies is the incorporation of functional building blocks, which can afford a synergic effect with MOFs. As far as catalytic applications are concerned, polyoxometallates (POMs) are well-known heterogeneous catalysts, for either acid or oxidation reactions.[9] The immobilization of POMs within the pores of a MOF can be seen as a way to obtain a well-defined solid with accessible catalytically active species. Structures of coordination polymer networks, mostly synthesized under mild and hydrothermal conditions, with POMs immobilized through host–guest interactions, have been recently reviewed.[10] In 2005, Férey et al. first described the encapsulation of Keggin-type POMs within the pores of the chromium terephthalate MIL-101 MOF.[11] In 2008, Kholdeeva and co-workers presented that MIL-101 adsorbing a single titanium $[(PW_{11}TiO_{40})^{5-}]$ or cobalt $[PW_{11}CoO_{39})^{5-}]$ atom inside can be used as a good heterogeneous selective-oxidation catalyst for the liquid-phase allylic oxidation of cyclohexene and α-pinene and the epoxidation of caryophyllene.[12] Subsequently, Gascon described a catalyst formed via the one-pot synthesis of MIL-

Received: December 14, 2011
Published: April 9, 2012

   dx.doi.org/10.1021/ic202685e | *Inorg. Chem.* 2012, 51, 5118–5127

101(Cr)-incorporating POMs, which showed remarkable activity for the Knoevenagel condensation of benzaldehyde with ethyl cyanoacetate and for acid-catalyzed reactions.[13] Recently, Liu et al. also displayed two host−guest materials constructed by POMs within a copper trimesate MOF and used as heterogeneous catalyst for the hydrolysis of carboxylic esters[14] and dimethyl methyphosphonate (DMMP).[15]

Inspired by the above-mentioned work of MOFs in catalysis, in our quest to gain more insight into the function of POM/MOFs as heterogeneous catalysts, we have focused our attention on a new strategy to address the problems of exploring efficient catalysts for hydrolysis of phosphate diesters. As a continuation of our previous work,[16] phosphotungstate was selected as the polyacid, because of their well-defined framework and polyacidic sites, Lewis acidity of Ln^{3+} and Zn^{2+} ions were selected as connectors, and 4,4′-bipyridine-*N*,*N*′-dioxide (dpdo) was selected as the longer spacer ligand for its excellent hard acid and small steric size to construct robust MOFs. In this strategy, the host−guest assembly of MOFs and solid polyacids may lead to a well-defined POM/MOFs materials that are easily accessible for activating the phosphodiester linkage and meanwhile enable facile recovery and reuse of the resulting hybrid catalysts. In this way, a series of new POM/MOFs hybrids are prepared through a one-step hydrothermal reaction, denoted as $\{[Eu_4(dpdo)_9(H_2O)_{16}PW_{12}O_{40}]\}(PW_{12}O_{40})_2$ $(dpdo)_3{\cdot}Cl_3$ (**1**); $\{[ZnNa_2(\mu\text{-}OH)(dpdo)_4(H_2O)_4][PW_{12}O_{40}]\}{\cdot}3H_2O$ (**2**); $\{Zn_3(dpdo)_7[PW_{12}O_{40}]_2{\cdot}3H_2O$ (**3**); and $[Ln_2H(\mu\text{-}O)_2(dpdo)_4(H_2O)_2][PW_{12}O_{40}]{\cdot}3H_2O$ (Ln = Ho (for **4**) and Yb (for **5**), respectively). Catalyses of hydrolytic cleavage of BNPP of these new POM/MOFs suggest a high catalytic activity and hydrolytic stability, and the precise requirements for their further use as material building blocks and/or as catalysts in hydrolytic cleavage of BNPP reactions. In this work, particular attention is also devoted to a comparison of the activity of the different metal ions in order to elucidate the most promising strategies that can be employed to obtain effective catalysts.

EXPERIMENTAL SECTION

General Methods and Materials. Elemental analyses (C, H, and N) were performed on a Perkin−Elmer Model 240C elemental analyzer. IR spectra were obtained from a solid sample palletized with KBr on Nicolet 170 SXFT-IR spectrometer in the range of 400−4000 cm^{-1}. ^{31}P NMR spectra were recorded on a Bruker Avance 300 spectrometer and on a Bruker Avance 400 spectrometer. Trimethyl phosphate was used as a 0 ppm ^{31}P reference. Fluorescence spectra were recorded on an Edinburgh Model FS920 luminescence spectrometer.

Syntheses. All reagents were used as purchased without further purification. $H_3[PW_{12}O_{40}]{\cdot}xH_2O$,[17] dpdo,[18] and BNPP[19] were prepared according to the literature methods and were characterized by infrared (IR) spectroscopy and mass spectroscopy (MS).

Preparation of $\{[Eu_4(dpdo)_9(H_2O)_{16}PW_{12}O_{40}]\}(PW_{12}O_{40})_2{\cdot}(dpdo)_3{\cdot}Cl_3$ *(**1**).* A mixture of $H_3PW_{12}O_{40}{\cdot}7H_2O$ (60 mg, 0.02 mmol), $Eu(NO_3)_3{\cdot}9H_2O$ (50 mg, 0.1 mmol), dpdo (37.6 mg, 0.2 mmol), piperazine (8.6 mg, 0.1 mmol) in mixed water (4 mL), and alcohol(4 mL) was stirred and its pH value was adjusted to 3.1 with 1 M HCl. The resulting suspension was sealed in a 25-mL Teflon-lined reactor and kept at 130 °C for three days. After cooling the autoclave to room temperature, pale yellow block single crystals of **1** were separated, washed with water, and air-dried (40% yield based on $H_3[\alpha\text{-}PW_{12}O_{40}]{\cdot}7H_2O$). Elemental analysis (%) calcd $C_{120}H_{128}N_{24}Cl_3O_{160}P_3W_{36}Eu_4$: C, 12.12; N, 2.83; H, 1.09; Found: C, 12.02; N, 2.94; H, 1.27. IR (KBr): four characteristic asymmetric vibrations resulting from heteropolyanions with the Keggin structure: $\upsilon(W{=}O_t)$ (923 cm^{-1}), $\upsilon(W{-}O_b)$ (887 cm^{-1}), $\upsilon(W{-}O_c)$ (797 cm^{-1}), and $\upsilon(P{-}O_a)$ (1071 cm^{-1}); four characteristic vibrations resulting from dpdo molecules, namely, υ(N−O) (1225 cm^{-1}), υ(ring) (1474 cm^{-1}), δ(C−H, in plane) (1180 cm^{-1}), and δ(N−O) (841 cm^{-1}).

Preparation of $\{ZnNa_2(\mu\text{-}OH)(dpdo)_4(H_2O)_4[PW_{12}O_{40}]\}{\cdot}3H_2O$ *(**2**).* A mixture of $H_3PW_{12}O_{40}{\cdot}7H_2O$ (60 mg, 0.02 mmol), $Zn(ClO_4)_2{\cdot}6H_2O$ (45 mg, 0.12 mmol), dpdo (18.8 mg, 0.1 mmol) in mixed water (4 mL), and alcohol (2 mL) was stirred and its pH value was adjusted to 6.0 with 1 M NaOH. The resulting suspension was sealed in a 25-mL Teflon-lined reactor and kept at 130 °C for four days. After cooling the autoclave to room temperature, colorless block single crystals of **2** were separated, washed with water, and air-dried (48% yield based on $H_3[\alpha\text{-}PW_{12}O_{40}]{\cdot}7H_2O$). Elemental analysis (%): Calcd $C_{40}H_{47}N_8O_{56}PW_{12}ZnNa_2$: C, 12.37; N, 2.88; H, 1.22; Found: C, 12.24; N, 2.97; H, 1.17. IR (KBr): four characteristic asymmetric vibrations resulting from heteropolyanions with the Keggin structure: $\upsilon(W{=}O_t)$ (921 cm^{-1}), $\upsilon(W{-}O_b)$ (885 cm^{-1}), $\upsilon(W{-}O_c)$ (793 cm^{-1}), and $\upsilon(P{-}O_a)$ (1079 cm^{-1}); four characteristic vibrations resulting from dpdo molecules, namely, υ(N−O) (1217 cm^{-1}), υ(ring) (1471 cm^{-1}), δ(C−H, in plane) (1180 cm^{-1}), and δ(N−O) (885 cm^{-1}).

Preparation of $\{Zn_3(dpdo)_7\}[PW_{12}O_{40}]_2{\cdot}3H_2O$ *(**3**).* A mixture of $H_3PW_{12}O_{40}{\cdot}7H_2O$ (60 mg, 0.02 mmol), $Zn(ClO_4)_2{\cdot}6H_2O$ (37.2 mg, 0.1 mmol), dpdo (18.8 mg, 0.1 mmol) in mixed water (3 mL) and alcohol (3 mL) was stirred and its pH value was at 4.0 without adjustment. The resulting suspension was sealed in a 25-mL Teflon-lined reactor and kept at 120 °C for 3 days. After cooling the autoclave to room temperature, colorless block single crystals of **3** were separated, washed with water, and air-dried (38% yield based on $H_3[\alpha\text{-}PW_{12}O_{40}]{\cdot}7H_2O$). Elemental analysis (%): Calcd for $C_{70}H_{62}N_{14}O_{97}P_2W_{24}Zn_3$: C, 11.48; N, 2.68; H, 0.85; Found: C, 11.74; N, 2.76; H, 0.90. IR (KBr): four characteristic asymmetric vibrations resulting from heteropolyanions with the Keggin structure: $\upsilon(W{=}O_t)$ (980 cm^{-1}), $\upsilon(W{-}O_b)$ (894 cm^{-1}), $\upsilon(W{-}O_c)$ (807 cm^{-1}), and $\upsilon(P{-}O_a)$ (1081 cm^{-1}); four characteristic vibrations resulting from dpdo molecules, namely, υ(N−O) (1218 cm^{-1}), υ(ring) (1469 cm^{-1}), δ(C−H, in plane) (1177 cm^{-1}), and δ(N−O) (885 cm^{-1}).

Preparation of $[Ho_2H(\mu\text{-}O)_2(dpdo)_4(H_2O)_2][PW_{12}O_{40}]{\cdot}3H_2O$ *(**4**).* A mixture of $H_3PW_{12}O_{40}{\cdot}7H_2O$ (60 mg, 0.02 mmol), $Ho(NO_3)_3{\cdot}8H_2O$ (49.5 mg, 0.1 mmol), dpdo (18.8 mg, 0.1 mmol), piperazine (8.6 mg, 0.1 mL) in mixed water (4 mL), and alcohol (4 mL) was stirred and its pH value was adjusted to 3.5 with 1 M HCl. The resulting suspension was sealed in a 25-mL Teflon-lined reactor and kept at 130 °C for three days. After cooling the autoclave to room temperature, pale pink block single crystals of **4** were separated, washed with water and air-dried (58% yield based on $H_3[\alpha\text{-}PW_{12}O_{40}]{\cdot}7H_2O$). Elemental analysis (%): Calcd for $C_{40}H_{43}N_8O_{55}$ $PW_{12}Ho_2$: C, 11.77; N, 2.74; H, 1.06; Found: C, 11.72; N, 2.78; H, 1.12. IR (KBr): four characteristic asymmetric vibrations resulting from heteropolyanions with the Keggin structure: $\upsilon(W{=}O_t)$ (922 cm^{-1}), $\upsilon(W{-}O_b)$ (886 cm^{-1}), $\upsilon(W{-}O_c)$ (796 cm^{-1}), and $\upsilon(P{-}O_a)$ (1069 cm^{-1}); four characteristic vibrations resulting from dpdo molecules, namely, υ(N−O) (1228 cm^{-1}), υ(ring) (1472 cm^{-1}), δ(C−H, in plane) (1180 cm^{-1}), and δ(N−O) (841 cm^{-1}).

Preparation of $[Yb_2H(\mu\text{-}O)_2(dpdo)_4(H_2O)_2][PW_{12}O_{40}]{\cdot}3H_2O$ *(**5**).* The preparation of **5** was similar to that of **4**, except that $Ho(NO_3)_3{\cdot}8H_2O$ (50 mg, 0.1 mmol) was replaced by $Yb(NO_3)_3{\cdot}8H_2O$. In addition, the pH of the resulting solution was adjusted to 3.5 with 1 M HCl. Pale yellow colorless crystals suitable for X-ray diffraction (XRD) were collected by filtration and dried in air (54% yield, based on $H_3[\alpha\text{-}PW_{12}O_{40}]{\cdot}7H_2O$). Elemental analysis (%): Calcd for $C_{40}H_{43}N_8O_{56}PW_{12}Yb_2$: C, 11.68; N, 2.72; H, 1.05; Found: C, 11.74; N, 2.68; H, 1.11. IR (KBr): four characteristic asymmetric vibrations resulting from heteropolyanions with the Keggin structure: $\upsilon(W{=}O_t)$ (922 cm^{-1}), $\upsilon(W{-}O_b)$ (887 cm^{-1}), $\upsilon(W{-}O_c)$ (799 cm^{-1}), and $\upsilon(P{-}O_a)$ (1078 cm^{-1}); four characteristic vibrations resulting from dpdo molecules, namely, υ(N−O) (1225 cm^{-1}), υ(ring) (1475 cm^{-1}), δ(C−H, in plane) (1181 cm^{-1}), and δ(N−O) (841 cm^{-1}).

X-ray Crystallographic Analyses. Intensity data for **1**−**5** were collected on Bruker CCD Apex-II diffractometer with Mo Kα radiation (λ = 0.71073 Å) at 296 K. The structures of **1**−**5** were

dx.doi.org/10.1021/ic202685e | *Inorg. Chem.* 2012, 51, 5118−5127

Table 1. Crystallographic Data and Structural Refinements for Compounds 1−5

parameter	Value				
	1	2	3	4	5
empirical formula	$C_{120}H_{128}Cl_3Eu_4N_{24}O_{160}P_3W_{36}$	$C_{40}H_{47}N_8O_{56}PW_{12}ZnNa_2$	$C_{70}H_{62}N_{14}O_{97}P_2W_{24}Zn_3$	$C_{40}H_{43}N_8O_{55}PW_{12}Ho_2$	$C_{40}H_{43}N_8O_{56}PW_{12}Yb_2$
formula weight	11891.80	3884.26	7321.61	4082.70	4114.92
crystal system	triclinic	triclinic	triclinic	monoclinic	monoclinic
space group	$P1$	$P\bar{1}$	$P\bar{1}$	$C2/m$	$C2/m$
a [Å]	18.850(13)	11.9039(7)	12.5305(4)	19.319(6)	19.232(6)
b [Å]	20.116(14)	12.0321(7)	16.1251(5)	17.529(5)	17.416(5)
c [Å]	20.773(14)	13.2106(8)	16.4694(5)	11.725(4)	11.738(3)
α [deg]	65.069(8)	91.959(3)	97.541(2)	90	90
β [deg]	65.798(7)	96.980(3)	91.323(2)	105.998 (4)	105.990 (4)
γ [deg]	64.594(8)	95.566(2)	97.644(2)	90	90
V [Å^3]	6195(7)	1867.24(19)	3266.85(18)	3817(2)	3779.4(19)
Z	1	1	1	2	2
ρ_{calc} [g/cm^3]	3.188	3.455	3.719	3.555	3.606
μ [mm^{-1}]	17.783	18.860	21.705	20.176	20.758
No. of data/parameters	21176/1545	6503/568	11428/991	3420/315	3416/289
GOOF	1.015	1.011	1.080	1.007	1.048
R_1 [$I > 2\sigma(I)$]	0.0697	0.0957	0.0824	0.1090	0.1037
wR_2	0.1307	0.2650	0.2102	0.3474	0.2822

resolved by direct methods using the SHELXTL-97 program package.[20] The remaining atoms were found from successive full-matrix least-squares refinements on F^2 and Fourier syntheses. Lorentz polarization and multiscan absorption corrections were applied. No hydrogen atoms associated with the water molecules were located from the difference Fourier map. Positions of the hydrogen atoms attached to the carbon atoms were geometrically placed. All hydrogen atoms were refined isotropically as a riding mode using the default SHELXTL parameters. Crystallographic data and structural refinements for **1**−**5** are summarized in Table 1.

Catalysis. The catalytic cleavage reactions of BNPP were carried out heterogeneously in 2 mL H_2O using 10 mol % of crystalline samples of **1**−**5** respectively, BNPP 20.4 mg (0.06 mmoL) under stirring in glass tubes placed in an oil bath at 323 K. The cleavage of BNPP was followed by monitoring of the increasing in absorbance at 400 nm due to the formation of the *p*-nitrophenoxide anion. The reaction mixture was withdrawn at regular intervals to study the progress of the reaction. In a typical operation, 10 μL solution was taken out with the help of a microsyringe and then was injected into 3 mL of an EPPS buffer solution (pH 8.2). The monitoring continued for ∼10 days until the absorbance did not increase. The pseudo-first-order rate constants k_{obsd} (s^{-1}) for these reactions were determined as the slopes of semilogarithmic plots of reaction progress ($A_L - A$) against time, where A is the observed absorbance at 400 nm and A_L is the final absorbance at the end of the reaction. For all reactions, the values of k_{obsd} were found to be reproducible to ±5%. Meanwhile, BNPP cleavage progress was also monitored by ^{31}P NMR. During the course of the reaction, there are three ^{31}P NMR signals, corresponding to inorganic phosphate (δ 0.04), *p*-nitrophenyl phosphate (δ −4.81), and BNPP (δ −11.21).

RESULTS AND DISCUSSION

Syntheses. The reactivity of the reaction system including $H_3PW_{12}O_{40}$, $Ln(NO_3)_3$, or $Zn(ClO_4)_2$ and dpdo in the mixed solution of H_2O and C_2H_5OH under hydrothermal conditions has been investigated, leading to a series of hybrids polyoxometallate-incorporated metal-organic frameworks (POM/MOFs), with one-dimensional (1D) to three-dimensional (3D) structural configurations. Scheme 1 illustrates the formation conditions of the related POM/MOFs.

As we know, many factors such as pH value, reaction temperature, metal ions, and the ratio of metal ions/ligand can influence the synthesis of POMs−template host−guest materials. In this system, there are two main factors playing great roles in constructing the different structures. First, ion radius plays a major role in coordination configuration, for instance, the coordination number of Zn^{2+}(0.74 Å) is five or six, while that of Eu^{3+} (0.95 Å) in **1** and Ho^{3+} (0.89 Å) or Yb^{3+} (0.86 Å) is eight and seven, respectively. Second, the pH has great influence on the construction of multidimensional structural frameworks in our case; for example, **3** with a two-dimensional (2D) structure was prepared at a pH value of 4.0, whereas when the pH value was increased to 6.0, **2** with a 3D structure was obtained. In addition, the POMs play various roles in constructing these POM/MOFs. For example, in **1**, they serve as a template to create the porous structure, and in **2**, they act as bridging ligands bound to the metal sites via coordination bonds; however, they act as charge-compensating counterions in the open system of **3**−**5**.

Scheme 1. Formation Conditions of Polyoxometallate-Incorporated Metal-Organic Frameworks (POM/MOFs) 1−5

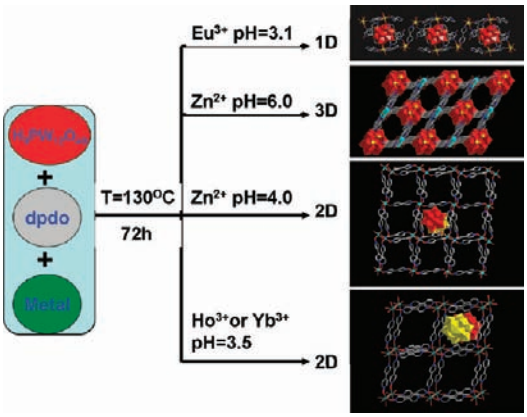

Structural Descriptions. All of this series of new POM/MOFs hybrids with 1D−3D structures consist of the typical Keggin anions $PW_{12}O_{40}^{3-}$. The polyoxoanion $PW_{12}O_{40}^{3-}$

dx.doi.org/10.1021/ic202685e | Inorg. Chem. 2012, 51, 5118−5127

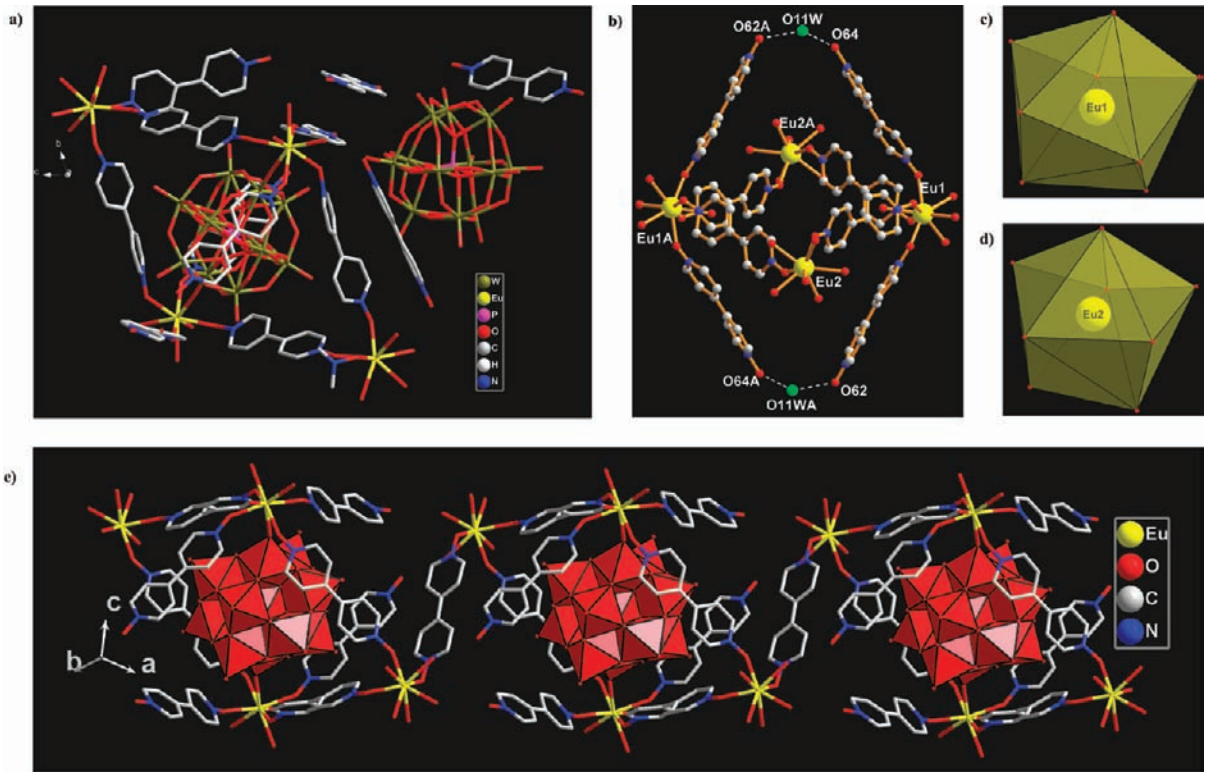

Figure 1. (a) Wires-and-sticks representation of **1**. The hydrogen atoms attached to carbon and nitrogen atoms are omitted for clarity. (b) Molecular structure of the $\{[Eu_4(dpdo)_8(H_2O)_{16}(H_2O)_2\}]$ cage, symmetry code: A = $-x$, $-y$, $2-z$. (c) The trigondodecahedra geometry of the Eu(1) cation. (d) The trigondodecahedra geometry of Eu(2) cation. (e) Polyhedral/wires-and-sticks representation of the 1D zigzag chain; the red polyhedron represents $PW_{12}O_{40}^{3-}$.

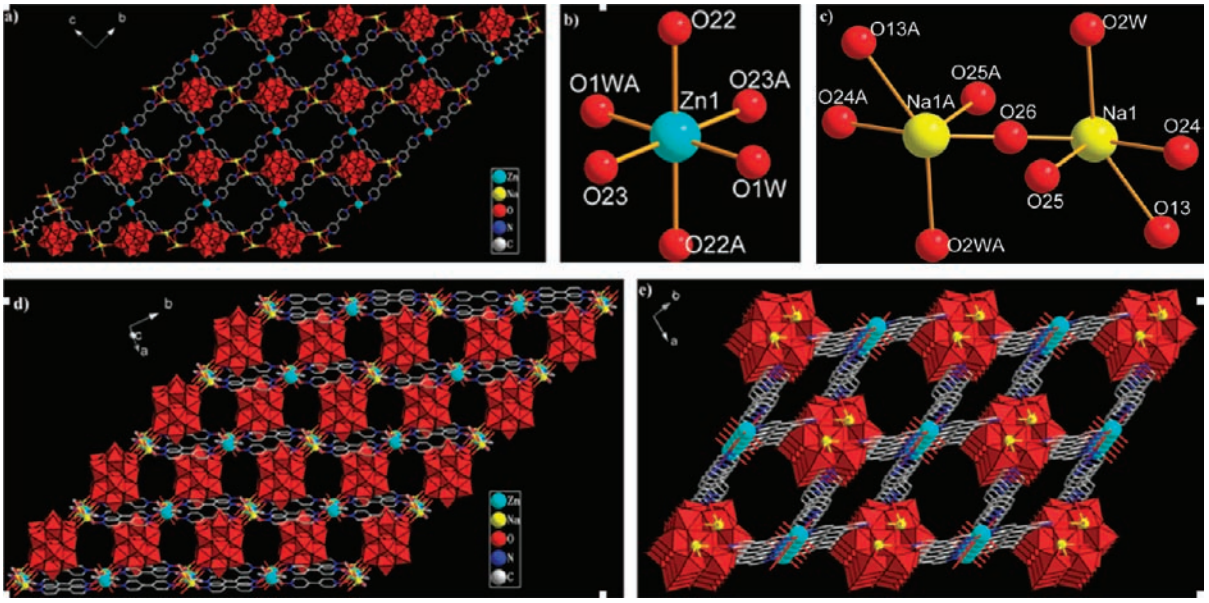

Figure 2. Views of structure **2**, showing (a) the 2D $[\{ZnNa_2(\mu\text{-}OH)(dpdo)_4(H_2O)_4\}\{PW_{12}O_{40}\}$ metal–ligand sheet in *bc* plane; (b) the coordinate environment of Zn^{2+} (symmetry code: A = $3-x$, $3-y$, $-z$); (c) the coordinate environment of Na^+ (symmetry code: A = $4-x$, $5-y$, $-z$); and (d and e) the 3D network composed of 2D $[\{ZnNa_2(\mu\text{-}OH)(dpdo)_4(H_2O)_4\}$sheets and polyanions from different axes.

exhibits a classical Keggin-type structure, in which the P atom is surrounded by a cube of eight oxygen atoms with each site of them half-occupied. The bond valence sum (BVS) values for W atoms indicate that all the oxidation states of W in **1**–**5** are +6.[21] The results are consistent with the formula of the title compound given by X-ray structure determination. Relevant W–O bond distances of the $PW_{12}O_{40}^{3-}$ can be grouped into three sets: W–O_t (terminal), W–$O_{b,c}$(bridge), and W–O_a (central).

Structural analysis display that **1** crystallizes in a triclinic space group $P\bar{1}$ and displays an infinite 1D chain (see Figure 1). Surprisingly, the 1D chains are constructed from a POM-based

dx.doi.org/10.1021/ic202685e | *Inorg. Chem.* 2012, 51, 5118–5127

lanthanide nanocage $\{[Eu_4(dpdo)_8(H_2O)_{16}PW_{12}O_{40}]\}_n^{9n+}$ as a secondary building block linked by bridging dpdo ligands. As can be seen from Figure 1b, four Eu^{III} ions connected by four bridged dpdo ligands, alternatively, consolidate the main skeleton of the nanocage $\{[Eu_4(dpdo)_8(H_2O)_{16}]\}^{12+}$. Both two crystallographically independent Eu1 and Eu2 centers are coordinated in distorted trigondodecahedra with oxygen atoms from coordinated water and dpdo molecules, respectively (see Figures 1c and 1d). The Eu(1)···Eu(1A) and Eu(2)···Eu(2A) separations in the equatorial plane are 15.2 and 22.2 Å, respectively. Two terminal dpdo ligands are toward one side of the rhombus, with the symmetry-related pair positioned on the other side. Each pair of terminal dpdo ligands positioned on one side forms hydrogen bonds with one water molecule to further complete the cagelike molecular cavity. The O···O separations of the hydrogen-bonding interaction are 2.68(4) and 2.57(4)Å for O(11W)···O(62) and O(11W)···O(64), respectively. One $PW_{12}O_{40}^{3-}$ anion bridging Eu(1) and Eu(1A) centers is found to fill the three-dimensional body with metal–ligand interactions between Eu(1) and the terminal oxygen atoms of the anion. Adjacent cages are linked together through coordination bonds between oxygen atoms of the bridging dpdo ligands and two Eu(2) atoms from different cages, generating a 1D ribbon composed of the nanocages (see Figure 1e). Adjacent ribbons are linked together through intermolecular hydrogen bonds and $\pi\cdots\pi$-stacking interactions in the crystal. Free $PW_{12}O_{40}^{3-}$ anions and solvent water molecules are found to fill the pores of the crystals. The solvent-accessible volume (SAV), calculated without including water molecules by PLATON[22] analysis, is 1056.6 $Å^3$, which is 17.1% of the unit-cell volume. In **1**, Eu(1) and Eu(2) are coordinated with three and five water molecules, respectively. The coordination geometry of the lanthanide ions is very consistent with that of the DNA-Foot printing active cyclen-based lanthanide complexes.[23] The water molecules occupy several coordination sites and have the potential to act as removable labile ligands, allowing for substrate binding and the simultaneous provision of a metal-bound nucleophile. Meanwhile, the Lewis acidity of lanthanide ion Eu(1) is enhanced by coordinated $PW_{12}O_{40}^{3-}$ directly; thus, compound **1** has the potential to exhibit excellent catalytic properties of hydrolysis for modes of natural phosphate esters.

Compound **2** crystallizes in a triclinic space group $P\bar{1}$. The structure of **2** is shown in Figure 2, which can be viewed as an adjacent four-connected 2D structure of $[\{ZnNa_2(\mu\text{-OH})(dpdo)_4(H_2O)_4\}^{3n+}$ connected with $[PW_{12}O_{40}]^{3-}$ through the direct coordination into a 3D structure framework. One of the most interesting structural features of this compound is that the $PW_{12}O_{40}^{3-}$ anions as bridging links connected with two diagonal Na^+ from two adjacent 2D sheets by terminal oxygen O(13) atoms, thus forming a 3D infinite network with free diameters of ca. 21 × 14 Å, and the pores accommodated the Keggin anions alternately (see Figure 2a). In $[\{ZnNa_2(\mu\text{-OH})(dpdo)_4(H_2O)_4\}^{3n+}$, each Zn^{2+} and $\{Na_2(\mu\text{-OH})\}^+$ acts as a four-coordination center located at the diagonal position of the 2D sheet. Zn^{2+} is coordinated in a distorted octahedral geometry by four oxygen atoms from four dpdo ligands (with the Zn–O bond distances varying from 2.04(3) Å to 2.14(3) Å) and two water molecules with Zn(1)–O(1W) bond distance being 2.06(3) Å (see Figure 2b). Each identical Na^+ unit is connected by sharing an oxygen atom to form binuclear secondary building units (SBUs), which act as pseudo-four-connected nodes (see Figure 2c). The five-coordinate Na^+ adopts a seriously distorted trigonal-bipyramidal geometry, which is coordinated by two O atoms from two dpdo molecules [Na(1)–O: 2.65(3)–2.88(3) Å] and a bridging oxygen O26 [Na(1)–O(26): 2.04(14) Å] building a trigonal plane and O2W [Na(1)–O(2W): 2.77(7) Å] and a terminal oxygen O13 [Na(1)–O(13): 2.74(3) Å] occupying the apical position. In comparison with that of static incorporation of the metal–organic unit and POMs into a 3D structure, the approach of constructing POM/MOFs through coordination linking does not only provide a convenient synthetic route to porous POMs-based materials, but also results in higher stability and catalyst activity. As we known, catalyst modification and fixation are the keys of the application of heterogeneous catalysis.

Compound **3** crystallizes in a triclinic space group $P\bar{1}$ and displays a novel infinite 2D sheet with unusual square voids constructed from alternative mono strand $\{Zn(dpdo)_2\}$ and double strands$\{Zn_{0.5}(dpdo)_2\}$, which are linked by two bridging dpdo molecules (Figure 3). Different from the case in **1** and **2**,

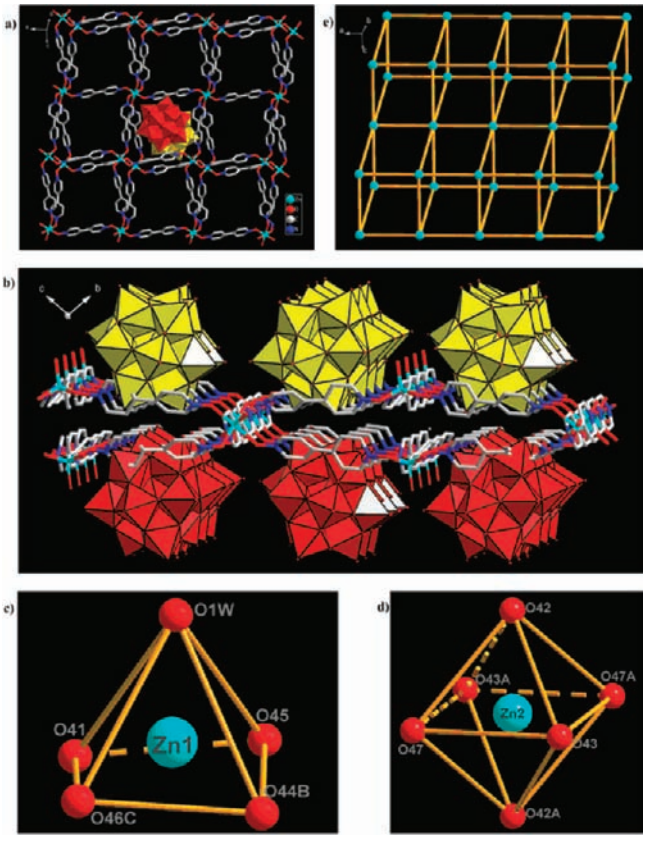

Figure 3. (a) View of the 2D framework of **3** in the *ab* plane. (b) View of the **3** along the *a*-axis. (c) Square-pyramid geometry of $Zn(1)^{2+}$ cation. (d) The octahedral geometry of $Zn(2)^{2+}$ cation, the symmetry transformation: A = 1 − *x*, 1 − *y*, −*z*; B = *x*, 1 + *y*, −1 − *z*; C = 1 + *x*, *y*, *z*. (e) Schematic representation of the connected net; the turquoise balls represent Zn nodes, and the bonds represent ligands.

the Keggin $PW_{12}O_{40}^{3-}$ entities function as counteranions locating on the sides of the 2D MOF framework by electrostatic interaction. The relatively small size of the cavity might be a reason why embedding two $PW_{12}O_{40}^{3-}$ anions simultaneously in the cavity may be difficult. Two crystallographically unique Zn^{2+} cations in **3** display different coordinated configurations. The five-coordinate Zn(1) atom adopts a square-pyramid geometry, which is coordinated by

dx.doi.org/10.1021/ic202685e | *Inorg. Chem.* 2012, 51, 5118–5127

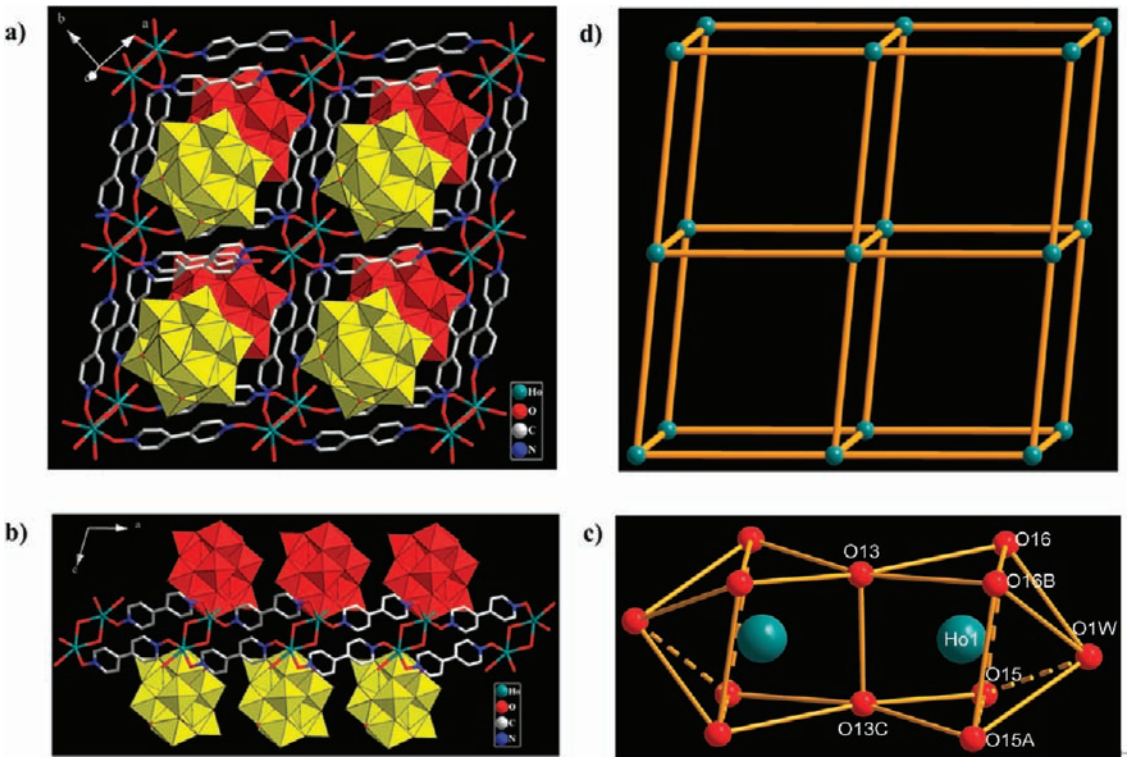

Figure 4. (a) View of the 2D framework of **4** in the *ab*-plane. (b) View of the **4** along the *b*-axis. (c) The $\{HoO_{10}\}$ dimer with single-capped trigonal prism geometry of $Ho(1)^{3+}$ cation, the symmetry transformation: A = *x*, −*y*, *z*; b = −0.5 + *x*, 0.5 + *y*, *z*; C = 1 − *x*, *y*, 3 − *z*. (d) Schematic representation of the four-connected net; the teal balls represent Ho nodes.

four O atoms from four molecules [Zn(1)−O: 1.966(10)−2.051(9) Å] building a basal plane and one O1W atom [Zn(1−O): 1.959(12) Å] occupying the apical position. The six-coordinate Zn(2) atom is only one-half occupied and resides in the distorted octahedral geometry, which is defined by four O atoms from four dpdo ligands [Zn(2)−O: 2.034(9)−2.202(9) Å] building the equatorial plane, O42 and O42A (1 − *x*, 1 − *y*, −*z*) atoms from another two dpdo units [Zn(2)−O(42): 2.074(10) Å] lying on the polar sites of the octahedron. It is noteworthy that there are no direct actions between two half-occupied Zn^{2+} cations, and the linkers are not well-paralleled.

Compounds **4** and **5** are basically isostructural and all crystallize in the monoclinic space group $C_{2/m}$, and their molecular structures are all unique 2D bilayer sheets with square voids constructed by binuclear rare-earth clusters as secondary building units (SBUs). The structures of compound **4** and **5** are composed of 2D bilayers of $[Ln_2H(\mu\text{-}O)_2(dpdo)_4(H_2O)_2]_n^{3n+}$(Ln = Ho or Yb), Keggin $PW_{12}O_{40}^{3-}$ polyanions and water molecules (Figure 4). Similar to **3**, the influence of the $PW_{12}O_{40}^{3-}$ anions as a noncoordinating anionic template in the construction of these structures is evident. The $PW_{12}O_{40}^{3-}$ anions locate on each side of the 2D sheets rather than penetrate them, perhaps because of the size limits of the square units (see Figure 4b).

Here, only take **4**, for example, to describe the structure in detail. The structural unit of **4** consists of one $PW_{12}O_{40}^{3-}$ anion, one coordination cation $[Ho_2H(\mu\text{-}O)_2(dpdo)_4(H_2O)_2]^{3+}$ and three water molecules of crystallization. $Ho(1)^{3+}$ cation is in a distorted single-capped trigonal prism geometry (Figure 4c), defined by four oxygen atoms from four dpdo ligands [Ho(1)−O: 2.305(8)−2.414(7) Å], two oxygen atoms from cocoordinated to Ho(2) [Ho(1)−O: 2.442(8) Å] and one terminal water ligand [Ho(1)−O1W: 2.319(8)−2.351(7) Å]. In the coordination configuration of $Ho(1)^{3+}$ cation, the O13, O16, and O16B group and the O13C, O15, and O15A group constitute the two bottom planes of the trigonal prism with the dihedral angle for the two bottom surfaces of 7.8°, and the distances between Ho(1) atom and the two bottom planes are 1.635 and 1.388 Å, respectively. The O1W is capped on the rectangle formed by O15, O15A, O16, and O16B group with a distance of 1.121 Å. The $\{Ho_{0.5}O_5\}_2$ dimer is formed by two one-half Ho polyhedra sharing edges with an Ho(1)···Ho(2) separation of 3.732(1) Å and then connect to each other through two dpdo groups forming a chain of SBUs along the *a*-axis (see Figure 4b). In the dimer, each one-half occupied Ho^{3+} acts as a four-connected node connected with dpdo ligands to form a 2D noninterwoven 4,4′-net having a cross section of ~17.5 Å × 19.3 Å (not considering the van der Waals radii of oxygen atoms). The noncoordinated H_2O molecules are incorporated in the framework. The solvent-accessible volume (SAV) calculated without including water molecules by PLATON analysis is 228.5 $Å^3$, which is 6.0% of the unit-cell volume. Although all compounds **3**−**5** display 2D infinite sheets, most differences are deserved to attention. In contrast to *edge-sharing* single-capped trigonal prism geometry generated between one-half occupied Ln^{3+} in **4** and **5**, there is less possible formation of edge-sharing in the Zn-MOF. This may be due to the Ho^{3+} (0.89 Å) and Yb^{3+}(0.86 Å) ions with larger ionic radii have higher coordination numbers (six to eight) than Zn^{2+} (0.74 Å), whose coordination number is general four or six.

Compared with the materials reported by Liu,[14] one difference deserve emphasis: in $[Cu_2(btc)_{4/3}(H_2O)_2]_6[H_nXM_{12}O_{40}]$ $(TMA)_2$ materials, they possess two kinds of pores, and only one type of pore is occupied by the POMs, with the other being partially filled with water molecules

dx.doi.org/10.1021/ic202685e | *Inorg. Chem.* 2012, 51, 5118−5127

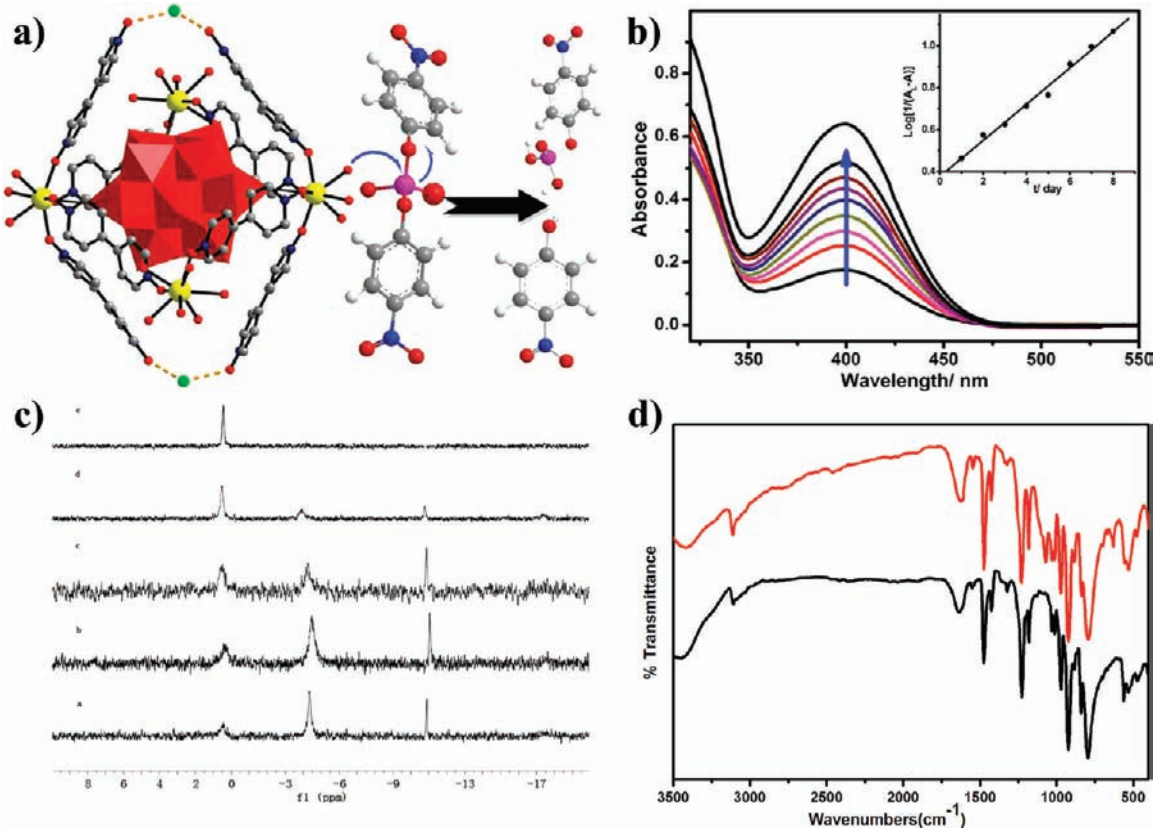

Figure 5. (a) Graphical representation for hydrolytic cleavage of BNPP by compound **1**. (b) Family of UV−visible absorbance spectra of a 4-nitrophenoxide anion formed from the cleavage of BNPP in H_2O at 50 °C. Inset: Kinetic plot of hydrolysis of BNPP using compound **1** as the catalyst. A is the observed absorbance, and A_L is the final absorbance at the end of the reaction. (c) ^{31}P NMR spectra of a H_2O solution containing equimolar amounts of BNPP and 1 (50 mM, pH 4.0, T = 50 °C, using $(CH_3)_3PO$ as a 0 ppm reference) measured after 1 day (spectrum a), 2 days (spectrum b), 4 days (spectrum c), 8 days (spectrum d), and 10 days (spectrum e) after mixing. Inorganic phosphate (δ 0.04), *p*-nitrophenyl phosphate (δ −4.81), BNPP (δ −11.21). (d) The IR spectrum comparison between before (black) and after (red) three catalysis treatments of **1**.

Table 2. Rate Constants and Half-Life Time of Hydrolysis with Compounds 1−5

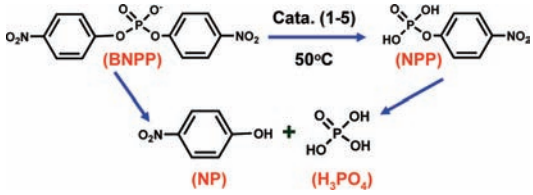

	1(Eu)	2(Zn)	3(Zn)	4(Ho)	5(Yb)
k_{obs}	$1.00(\pm0.04) \times 10^{-6}$	$6.74(\pm0.22) \times 10^{-7}$	$8.80(\pm0.30) \times 10^{-7}$	$7.57(\pm0.36) \times 10^{-7}$	$1.19(\pm0.07) \times 10^{-6}$
$t_{1/2}$	6.93×10^5	1.03×10^6	7.88×10^5	9.15×10^5	5.82×10^5

and TMA^+ cations. However, in all of our materials, the pores of the coordination polymers are totally blocked by the bulky POM anions. To some extent, the pore materials are more promising candidates for catalytic applications. In next work, we will pay attention to investigating the factors that influence the MOF structures.

Cleavage of a DNA-Model Phosphodiester. DNA is obviously the most interesting substrate for hydrolytic agents. However, because of its polyanionic nature, DNA is tremendously resistant to hydrolysis.[24] As a result, it is very difficult to perform any mechanistic investigation on this substrate. The most popular DNA model is BNPP, notwithstanding the presence of two good leaving groups, is still quite resistant to hydrolytic cleavage; the rate of spontaneous hydrolysis in water at pH 7 and 25 °C has been estimated to be 1.6×10^{-11} s^{-1}, which corresponds to a half-life of more than 1300 years. Recently, various sophisticated catalysts such as well-defined molecular catalysts, biomimetic catalysts related to the heme-enzyme of cytochrome P-450 and the nonheme enzyme of methane monooxygenase, and isolated single-site heterogeneous catalysts with high specific reactivity for the cleavage of a DNA-model phosphodiester reactions have been sufficiently reported.[2] In previous work, we first explored POM/MOFs as a heterogeneous catalyst for BNPP cleavage. By making a comparison under different pH conditions, k_{obsd} is only slightly decreased with change of the pH of the solution, and the fastest cleavage is observed at pH 4.0. Herein, the catalysis is carried under the optimum conditions. Cleavage of BNPP was followed by monitoring of the increasing in absorbance at 400 nm due to formation of a 4-nitrophenoxide

dx.doi.org/10.1021/ic202685e | *Inorg. Chem.* 2012, 51, 5118−5127

anion, generally, and no obvious pH change was observed during the catalytic processes. The heterogeneous catalysis of compounds **1**−**5** for phosphodiester bond cleavage is evidenced.

First, the compound **1** was taken to the hydrolysis experiment. As can be seen in Figure 5, a plot of the reaction progress $\log[1/(A_L - A)]$ against time fits well with the pseudo-first-order rate equation, giving a rate constant k_{obsd} of 1.00 (±0.04) × 10^{-6} s^{-1}, and a half-life time of 6.93 × 10^5 s.[25] Furthermore, BNPP cleavage progress was also monitored by ^{31}P NMR. During the course of the reaction, there are three ^{31}P NMR signals, corresponding to inorganic phosphate (δ 0.04), *p*-nitrophenyl phosphate (δ −4.81), and BNPP (δ −11.21) (Figure 5c). At the end of the reaction, only the signal due to inorganic phosphate remains. A plot of the reaction progress conversion rate against time also fits well with the pseudo-first-order rate equation. The k_{obsd} for the BNPP hydrolysis calculated by integrating the ^{31}P NMR signal of the initial BNPP-1 complex afforded virtually the slightly higher value (7.28 × 10^{-6} s^{-1}) than k_{obsd} calculated by measuring the UV absorbance of *p*-nitrophenol (1.00 × 10^{-6} s^{-1}).

In the same way, others compounds (**2**−**5**) were also applied to BNPP hydrolysis, as can be seen from Table 2; slight changes in the BNPP cleavage rate catalyzed by **1**−**5** are found, and the Eu^{3+} and Yb^{3+} complexes catalysis phosphate diesters with rate constants k_{obs} of approximately the same order of magnitude and higher than that of Zn^{2+} complexes. The results indicate that metal ion radius ($r(Ln^{3+}) > r(Zn^{2+})$) and coordination model or Ligand field stabilization energy (LFSE) determined the BNPP catalytic cleavage rate. In addition, for lanthanide complexes, the k_{obs} increases as the hydrolysis tendency of the metal ion (as reflected in the p*K*a of the coordinated water)[26] increases, which is decided by the ionic potential (¢) of metal ions. The results indicate that the k_{obs} of MOF containing Eu^{3+}(1.00 × 10^{-6}) and Yb^{3+}(1.19 × 10^{-6}) is compatible with the ¢ value (¢(Eu^{3+}) 3.16 < ¢(Yb^{3+}) 3.50). However, there is an abnormality for the MOF containing Ho^{3+} **4** and Eu^{3+} **1**, in that ¢(Ho^{3+}) 3.36 is larger than ¢(Eu^{3+}) 3.16, while the rate constants k_{obs} of **4** is smaller than that of **1**. It may be due to the fact that the Lewis acidity of lanthanide ion Eu(1) is enhanced by coordinated $PW_{12}O_{40}^{3-}$ directly. The catalytic activity for BNPP with a certain number of moles of the heterogeneous catalyst can match those of prior studies using a similar number of moles of a homogeneous catalyst,[27] indicative of a rapid acceleration of the cleavage of BNPP. More significantly, the removal of MOF **1** by filtration after only 5 d completely shut down the reaction, affording only 5% additional conversion upon stirring for another 5 d. These experiments unambiguously demonstrate that MOF **1** is a true heterogeneous asymmetric catalyst. The crystals of compounds **1**−**5** were easily isolated from the reaction suspension by filtration alone and reused three times, displaying only a slight decrease in activity. The exact index of the IR of compound **1** after the catalytic reaction supports that the crystallographic data characteristic of compound **1** are maintained directly. (See Figure 5d.)

The mechanism of the metal-catalyzed hydrolysis of DNA model phosphate diesters has been investigated in great detail,[3a] in the case of monometallic complexes, the commonly accepted mechanism involves the nucleophilic attack of a water (or hydroxide ion) oxygen at the phosphorus to give a five-coordinate phosphate intermediate (or transition state); the subsequent expulsion of one alcoholic (or alkoxide) fragment provides the products. Substrate structure, either the nucleophilic attack or the breakdown of the intermediate, can be rate-limiting. The hydrolysis is assisted by metal ions in different ways. The main steps are the acid dissociation of a metal-coordinated water molecule, the coordination of the substrate to the metal ion, and the nucleophilic attack of the metal-bound hydroxide on the substrate. As far as the structures of **1**−**5** are concerned, their catalyzed hydrolysis of BNPP can be observed in the following monometallic-catalyzed mechanism.

As we know, in all types of MOFs used in catalysis, three different parts can be clearly differentiated: (i) the metallic component, (ii) the organic ligand, and (iii) the pore system. From the mechanism of the metal-catalyzed hydrolysis of BNPP, the metallic ions play a key role in the catalysis cleavage of BNPP. We can deduce, from a structural point of view, that the BNPP cleavage is benefited by the large size and high coordination numbers of Ln^{3+} and Zn^{2+}, and the small steric size of the dpdo ligand. The presence of water molecules as the labile ligands allows for substrate binding and the simultaneous provision of a metal-bound nucleophile. There is only one type of metal center in each the MOF **4** and **5**, which simultaneously acts as a structural building component and a catalytic active site. In MOF **1**, there are two crystallographically independent centers: Eu1 and Eu2. The Eu(1) centers are bridged by one $PW_{12}O_{40}^{3-}$ anion by the terminal oxygen atoms of the anion, the Lewis acidity of Eu(1) is increased which resulted in higher rate constants (k_{obsd}) than that of Ho^{3+} complexes. The $PW_{12}O_{40}^{3-}$ anions, with their strong Brønsted acidity, play a synergistic action as solid acids in the catalysis cleavage of BNNP. Since, in all of these materials, the pores of the coordination polymers are totally blocked by the bulky POM anions, it is difficult for BNNP to approach the free POMs.

Photoluminescence Properties. The solid-state luminescent properties of **1**, **4**, and **5** were measured at room temperature. The results reveal that only **1** shows obvious luminescent phenomena (Figure 6). When the Eu^{III}-based

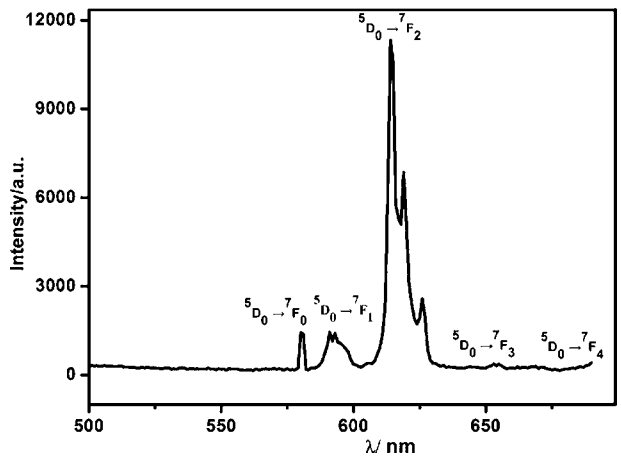

Figure 6. Solid-state emission spectrum of **1** (λ_{ex} = 330 nm) at room temperature.

compound **1** was excited at 350 nm, **1** displays intense red luminescence and exhibits the characteristic luminescent bands at 581, 591, 614, 653, 690 nm via the ligand-to-metal energy-transfer mechanism, corresponding to the transitions from the $^5D_0$ state to the ^7F_J (J = 0−4) levels, respectively.[28,29] It is known that lanthanide luminescence is demonstrated to be very

dx.doi.org/10.1021/ic202685e | *Inorg. Chem.* 2012, 51, 5118−5127

sensitive to the local environments around the lanthanide center.[30] The appearance of the symmetry-forbidden emission $^5D_0 \rightarrow {}^7F_0$ at 581 nm indicates that Eu^{3+} cations in **1** occupy sites with low symmetry and have no inversion center.[29,31] This is further confirmed by the fact that the $^5D_0 \rightarrow {}^7F_2$ transition is much more intense than the $^5D_0 \rightarrow {}^7F_1$ transition, which is consistent with the result of the single-crystal X-ray analysis that Eu^{3+} cations have distorted trigondodecahedra geometry.

CONCLUSIONS

In summary, we have developed a new strategy to prepare a series of crystalline materials with diversity structures from one-dimensional (1D) to three-dimensional (3D) POM/MOFs through hydrothermal reaction and first explored them in the hydrolysis of phosphodiester bond cleavage. In this work, the cleavage of phosphodiester catalyzed by compounds **1**−**5** as heterogeneous acid catalysts, with high activity, suggesting a pseudo-first-order hydrolytic cleavage reaction in an aqueous solution, were extensively developed. The results confirmed that these compounds have great potential as heterogeneous catalysts because they possess some excellent characteristics, such as unambiguous X-ray crystallography, good dispersion of POMs at the molecular level, high immobilization of POMs, highly stable crystalline framework, and others, which allows for catalyst recycling. The approaches presented here show that designing a novel material with a cooperative function based on the MOFs and POMs is a promising strategy. The kinetic and theoretical studies are in progress to unequivocally identify the active species and to elucidate the mechanisms involved. Despite the many achievements in MOF development, there are still tremendous opportunities for further exploration.

ASSOCIATED CONTENT

Supporting Information

Crystal data in CIF format. This information is available free of charge via the Internet at http://pubs.acs.org.

AUTHOR INFORMATION

Corresponding Author

*Tel.: (+86)-411-84986262. Fax: (+86)-411-84986261. E-mail: cyduan@dlut.edu.cn.

Notes

The authors declare no competing financial interest.

ACKNOWLEDGMENTS

This work was supported by the National Science Foundation of China (Grant No. 21025102).

REFERENCES

(1) (a) Weston, J. *Chem. Rev.* **2005**, *105*, 2151−2174. (b) Mancin, F.; Scrimin, P.; Tecilla, P.; Tonellato, U. *Chem. Commun.* **2005**, 2540−2548. (c) Yatsimirsky, A. K. *Coord. Chem. Rev.* **2005**, *249*, 1997−2011. (d) Liu, C.; Wang, M.; Zhang, T.; Sun, H. *Coord. Chem. Rev.* **2004**, *248*, 147−168. (e) Suh, J. *Acc. Chem. Res.* **2003**, *36*, 562−570. (f) Kimura, E.; Kikuta, E. J. *J. Biol. Inorg. Chem.* **2000**, *5*, 139−155.

(2) (a) Camargo, M. A.; Neves, A.; Bortoluzzi, A. J.; Szpoganicz, B.; Fischer, F. L.; Terenzi, H. A.; Serra, O. A.; Santos, V. G.; Vaz, B. G.; Eberlin, M. N. *Inorg. Chem.* **2010**, *49*, 6013−6025. (b) Nwe, K.; Andolina, C. M.; Morrow, J. R. *J. Am. Chem. Soc.* **2008**, *130*, 14861−14871. (c) Fanning, A. M.; Plush, S. E.; Gunnlaugsson, T. *Chem. Commun.* **2006**, 3791−3793. (d) Roigk, A.; Yescheulova, O. V.; Fedorov, Y. V.; Fedorova, O. A.; Gromov, S. P.; Schneider, H. J. *Org. Lett.* **1999**, *1*, 833−835.

(3) (a) Mancin, F.; Tecilla, P. *New J. Chem.* **2007**, *31*, 800−817. (b) Neverov, A. A.; Liu, C. T.; Bunn, S. E.; Edwards, D.; White, C. J.; Melnychuk, S. A.; Brown, R. S. *J. Am. Chem. Soc.* **2008**, *130*, 6639−6649.

(4) Yamamoto, Y.; Uehara, A.; Watanabe, A.; Aburatani, H.; Komiyama, M. *ChemBioChem* **2006**, *7*, 673−677.

(5) Komiyama, M.; Takeda, N.; Shigekawa, H. *Chem. Commun.* **1999**, 1443−1451.

(6) Heitbaum, M.; Glorius, F.; Escher, I. *Angew. Chem., Int. Ed.* **2006**, *45*, 4732−4762.

(7) (a) Bodsgard, B. R.; Burstyn, J. N. *Chem. Commun.* **2001**, 647−648. (b) Zaupa, G.; Prins, L. J.; Scrimin, P. *Bioorg. Med. Chem. Lett.* **2009**, *19*, 3816−3820.

(8) (a) Corma, A.; García, H.; Llabrés i Xamena, F. X. *Chem. Rev.* **2010**, *110*, 4606−4655. (b) Ranocchiari, M.; Bokhoven, J. A. v. *Phys. Chem. Chem. Phys.* **2011**, *13*, 6388−6396.

(9) (a) Mizuno, N.; Misono, M. *Chem. Rev.* **1998**, *98*, 199−217. (b) Mizuno, N.; Kamata, K.; Yamaguchi, K. *Top Catal.* **2010**, *53*, 876−893. (c) Dolbecq, A.; Dumas, E.; Mayer, C. R.; Mialane, P. *Chem. Rev.* **2010**, *110*, 6009−6048. (d) Hill, C. *J. Mol. Catal. A: Chem.* **2007**, 1−2. (e) Mizuno, N.; Misono, N. *Chem. Rev.* **1998**, *98*, 199−217. (f) Neumann, R. *Prog. Inorg. Chem.* **1998**, *47*, 317−339.

(10) (a) Zheng, S. T.; Zhang, J.; Li, X. X.; Fang, W. H.; Yang, G. Y. *J. Am. Chem. Soc.* **2010**, *132*, 15102−15103. (b) Yu, R.; Kuang, X. F.; Wu, X. Y.; Lu, C. Z.; Donahue, J. P. *Coord.Chem. ReV.* **2009**, *253*, 2872−2890. (c) Kuang, X. F.; Wu, X. Y.; Yu, R. M.; Donahue, J. P.; Huang, J. S.; Lu, C. Z. *Nature Chem.* **2010**, *2*, 461−465. (d) Yu, F.; Zheng, P. Q.; Long, Y. X.; Ren, Y. P.; Kong, X. J.; Long, L. S.; Yuan, Y. Z.; Huang, R. B.; Zheng, L. S. *Eur. J. Inorg. Chem.* **2010**, 4526−4531. (e) Knaust, J. M.; Inman, C.; Keller, S. W. *Chem. Commun.* **2004**, 492−493. (f) Wei, M. L.; He, C.; Hua, W.; Duan, C. Y.; Li, S.; Meng, Q. J. *J. Am. Chem. Soc.* **2006**, *128*, 13318−13319. (g) Wang, X.; Bi, Y.; Chen, B.; Lin, H.; Liu, G. *Inorg. Chem.* **2008**, *47*, 2442−2448.

(11) Férey, G.; Mellot-Draznieks, C.; Serre, C.; Millange, F.; Dutour, J.; Surble, S.; Margiolaki, I. *Science* **2005**, 2040−2042.

(12) (a) Maksimchuk, N. V.; Timofeeva, M. N.; Melgunov, M. S.; Shmakov, A. N.; Chesalov, Y. A.; Dybtsev, D. N.; Fedin, V. P.; Kholdeeva, O. A. *J. Catal.* **2008**, *257*, 315−323.

(13) Juan-Alcañiz, J.; Ramos-Fernandez, E. V.; Lafont, U.; Gascon, J.; Kapteijn, F. *J. Catal.* **2010**, *269*, 229−241.

(14) Sun, C. Y.; Liu, S. X.; Liang, D. D.; Shao, K. Z.; Ren, Y. H.; Su, Z. M. *J. Am. Chem. Soc.* **2009**, *131*, 1883−1888.

(15) Ma, F. J.; Liu, S. X.; Sun, C. Y.; Liang, D. D.; Ren, G. J.; Wei, F.; Chen, Y. G.; Su, Z. M. *J. Am. Chem. Soc.* **2011**, *133*, 4178−4181.

(16) Dang, D. B.; Bai, Y.; He, C.; Wang, J.; Duan, C. Y.; Niu, J. Y. *Inorg. Chem.* **2010**, *49*, 1280−1282.

(17) Rocchiccioli-Deltcheff, C.; Fournier, M.; Franck, R.; Thouvenot, R. *Inorg. Chem.* **1983**, *22*, 207−216.

(18) Jia, J. H.; Blake, A. J.; Champness, N. R.; Hubberstey, P.; Wilson, C.; Schröder, M. *Inorg. Chem.* **2008**, *47*, 8652−8664.

(19) Zhou, S. H.; Zeng, Z. J.; Li, X. Y.; Gao, Z. W. *Zhongguo Yaowu Huaxue Zazhi* **2001**, *11* (3), 172−173.

(20) Sheldrick, G. M. *SHELXTL97, Program for Crystal Structure Solution*; University of Göttingen: Göttingen, Germany, 1997.

(21) Brown, I. D.; Altermatt, D. *Acta Crystallogr., Sect. B: Struct. Sci.* **1985**, *41*, 244−247.

(22) Spek, A. L. *J. Appl. Crystallogr.* **2003**, *36*, 7−13.

(23) Lu, Z. L.; Liu, C. T.; Neverov, A. A.; Brown, R. S. *J. Am. Chem. Soc.* **2007**, *129*, 11642−11652.

(24) Williams, N. H.; Takasaki, B. K.; Wall, M. *Chin. Acc. Chem. Res.* **1999**, *32*, 485−493.

(25) Hydrolysis of BNPP in the absence of a metal complex was almost negligible, compared to that of the catalytic reaction; however, the final value of k_{obs} was also adjusted for the background cleavage.

(26) Burgess, J. *Metal Ions in Solution*; Wiley: New York, 1978; p 267.

(27) Takasaki, B. K.; Chin, J. *J. Am. Chem. Soc.* **1993**, *115*, 9337−9338.

(28) (a) Xia, J.; Zhao, B.; Wang, H. S.; Shi, W.; Ma, Y.; Song, H. B.; Cheng, P.; Liao, D. Z.; Yan, S. P. *Inorg. Chem.* **2007**, *46*, 3450−3458.

(29) (a) Li, Y.; Zheng, F. K.; Liu, X.; Zou, W. Q.; Guo, G. C.; Lu, C. Z.; Huang, J. S. *Inorg. Chem.* **2006**, *45*, 6308−6316. (b) Cheng, J. W.; Zheng, S. T.; Ma, E.; Yang, G. Y. *Inorg. Chem.* **2007**, *46*, 10534−10538.
(30) (a) Foster, D. R.; Richardson, F. S. *Inorg. Chem.* **1983**, *22*, 3996−4002. (b) Yanagida, S.; Hasegawa, Y.; Murakoshi, K.; Wada, Y.; Nakashima, N.; Yamanaka, T. *Coord. Chem. Rev.* **1998**, *171*, 461−480. (c) Yamada, T.; Shinoda, S.; Sugimoto, H.; Uenishi, J. I.; Tsukube, H. *Inorg. Chem.* **2003**, *42*, 7932−7937.
(31) (a) Bünzli, J. C. G.; Piguet, C. *Chem. Soc. Rev.* **2005**, *34*, 1048−1077. (b) Sun, Y. Q.; Zhang, J.; Chen, Y. M.; Yang, G. Y. *Angew. Chem., Int. Ed.* **2005**, *44*, 5814−5817.